

Advances in
**Physical Organic
Chemistry**

Volume 53





VOLUME FIFTY THREE

ADVANCES IN
PHYSICAL ORGANIC
CHEMISTRY

Academic Press is an imprint of Elsevier
125 London Wall, London, EC2Y 5AS, United Kingdom
The Boulevard, Langford Lane, Kidlington, Oxford OX5 1GB, United Kingdom
525 B Street, Suite 1650, San Diego, CA 92101, United States
50 Hampshire Street, 5th Floor, Cambridge, MA 02139, United States

First edition 2019

Copyright © 2019 Elsevier Ltd. All rights reserved.

No part of this publication may be reproduced or transmitted in any form or by any means, electronic or mechanical, including photocopying, recording, or any information storage and retrieval system, without permission in writing from the publisher. Details on how to seek permission, further information about the Publisher's permissions policies and our arrangements with organizations such as the Copyright Clearance Center and the Copyright Licensing Agency, can be found at our website: www.elsevier.com/permissions.

This book and the individual contributions contained in it are protected under copyright by the Publisher (other than as may be noted herein).

Notices

Knowledge and best practice in this field are constantly changing. As new research and experience broaden our understanding, changes in research methods, professional practices, or medical treatment may become necessary.

Practitioners and researchers must always rely on their own experience and knowledge in evaluating and using any information, methods, compounds, or experiments described herein. In using such information or methods they should be mindful of their own safety and the safety of others, including parties for whom they have a professional responsibility.

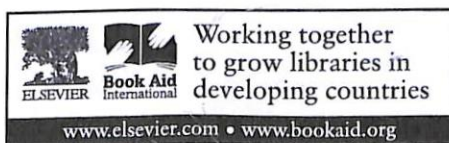
To the fullest extent of the law, neither the Publisher nor the authors, contributors, or editors, assume any liability for any injury and/or damage to persons or property as a matter of products liability, negligence or otherwise, or from any use or operation of any methods, products, instructions, or ideas contained in the material herein.

ISBN: 978-0-08-102900-8

ISSN: 0065-3160

For information on all Academic Press publications
visit our website at <https://www.elsevier.com/books-and-journals>

Publisher: Zoe Kruze
Acquisition Editor: Jason Mitchell
Editorial Project Manager: Leticia Lima
Production Project Manager: James Selvam
Cover Designer: Alan Studholme
Typeset by SPI Global, India



Contents

<i>Contributors</i>	<i>vii</i>
1. Computational asymmetric catalysis: On the origin of stereoselectivity in catalytic reactions	1
Sukriti Singh and Raghavan B. Sunoj	
1. Introduction	2
2. Asymmetric dearomative amination of β -naphthols	9
3. Pd-Catalyzed C–H Arylation	11
4. Desymmetrization of three-substituted oxetanes	13
5. Enantioselective heck matsuda arylation	15
6. Enantioselective synthesis of indoles	17
7. Asymmetric α -allylation of aldehydes	19
8. Summary and outlook	22
References	22
2. The transition state and cognate concepts	29
Iñaki Tuñón and Ian H. Williams	
1. Introduction	30
2. Conceptual power of the transition state	32
3. Glossary of terms	33
4. Computation and experiment for simple systems	42
5. Transition state for condensed systems: Concepts and simulations	50
6. Concluding remarks	62
Acknowledgments	64
References	64
3. Computational physical organic chemistry using the empirical valence bond approach	69
Yashraj Kulkarni and Shina Caroline Lynn Kamerlin	
1. Introduction	70
2. Theoretical background	71
3. Dissecting catalysis using the empirical valence bond approach	73
4. Using the empirical valence bond approach to understand linear free energy relationships in enzymatic reactions	77



Computational asymmetric catalysis: On the origin of stereoselectivity in catalytic reactions

Sukriti Singh, Raghavan B. Sunoj*

Department of Chemistry, Indian Institute of Technology Bombay, Mumbai, India

*Corresponding author: e-mail address: sunoj@chem.iitb.ac.in

Contents

1. Introduction	2
2. Asymmetric dearomative amination of β -naphthols	9
3. Pd-Catalyzed C–H Arylation	11
4. Desymmetrization of three-substituted oxetanes	13
5. Enantioselective heck matsuda arylation	15
6. Enantioselective synthesis of indoles	17
7. Asymmetric α -allylation of aldehydes	19
8. Summary and outlook	22
References	22

Abstract

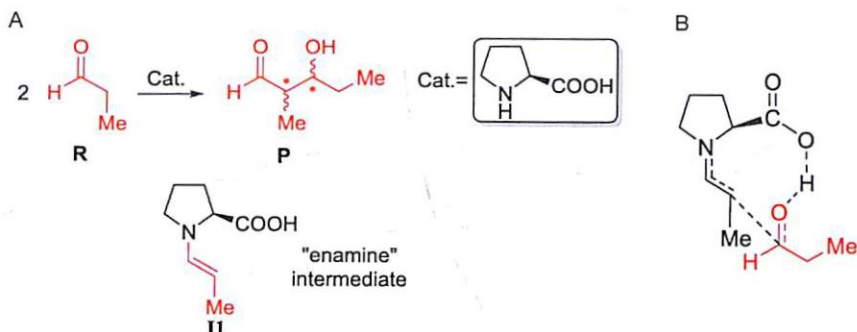
Molecular understanding of chemical reactivity has become progressively better with the advent of powerful computational methods. In the domain of computational catalysis, one strives to establish the identity of various intermediates and transition states involved along the catalytic pathways. Kinetic and thermodynamic details of such catalytic transformations are important to physical organic chemistry. Herein, we present a set of contemporary examples of asymmetric catalysis to demonstrate the power of modern computational tools toward establishing the origin of stereoselectivity. We demonstrate how enantio- and diastereo-selectivities in a range of important asymmetric reactions could be better understood by having knowledge of the stereocontrolling transition states. In particular, the critical role played by weak noncovalent interactions is the central theme of this article. A good number of examples provided here helped us convey how differential weak interactions between the stereocontrolling transition state render additional stabilization to the most preferred stereochemical mode of addition. Furthermore, we emphasize that such weak interactions could be exploited as an effective handle toward gaining better control over the stereochemical outcome of asymmetric reactions.



1. Introduction

Asymmetric catalysis has been witnessing a steady growth over the past few decades. Development of new protocols in asymmetric catalysis traditionally involves a lot of trial and error experimentation, predominantly centered around minor alterations on the catalyst. In such an approach, the reaction conditions are typically optimized with a set of other parameters such as temperature, additives, solvents, and so on, with the same or similar set of well performing substrates. One of the key goals in asymmetric catalysis is to gain predictable control over the stereochemical outcome of the reaction. In particular, accomplishing high enantioselectivity is of paramount importance. A chiral catalyst, bearing one or more elements of chirality, is employed in asymmetric transformations. The chiral catalyst, which provides the critical chiral environment for the reaction to take place, could engage directly by forming bonds with the reactant(s) and/or develop weak interactions with the reactant(s) without engaging in formal bond formation. Among these, the first mode of action of a catalyst is generally termed as a covalent mode of activation whereas a noncovalent activation pertains to the latter mode.

The covalent mode of asymmetric catalysis can be better understood by considering the following example, wherein an enamine (**II**) derived from one of the reactants serves as the nucleophile and the unactivated electrophilic partner will then react with the enamine (Scheme 1A). In this example, the stereogenic center of the catalyst bearing a carboxylic acid group is proximal to the enamine that participates in the C–C bond formation with the incoming electrophile. The facial preference of the enamine, i.e., whether the *si* or *re* prochiral face is energetically more preferred for the C–C bond formation would directly impact which enantiomer of the product would be generated. It is important to take note at this point that the origin of enantioselectivity could be rationalized by using a working hypothesis or a more quantitative model based on the structure and energies of a computed transition state. While a working hypothesis generally places an undue weight on steric protection to justify why one prochiral face is likely to participate in the bond formation over the other, it fails to provide insights on critical interactions (*vide infra*) in the stereocontrolling transition states.



Scheme 1 (A) Proline catalyzed asymmetric self aldol reaction between propanal and (B) qualitative transition state model.

Qualitative transition state models relying on steric interactions to rationalize the observed facial preference between the prochiral faces in the stereocontrolling step are the most widely found in current literature. The use of hydrogen bonding interactions between the catalyst and substrate(s) are also invoked in accounting for the observed enantioselectivity in asymmetric reactions such as proline catalyzed organocatalytic transformations (Scheme 1B). While such models based on certain obvious features of the chiral catalyst offer a simple working hypothesis, we note their inadequacies in capturing vital electronic interactions in the stereocontrolling transition states. Hence, we aim at emphasizing the importance of factors beyond the steric interaction models and provide molecular insights on enantio-controlling transition states in some of the most recent asymmetric transformations. The examples presented in the following sections encompass reactions catalyzed either by one chiral catalyst, such as a chiral organocatalyst, or by a dual catalytic combination involving one organo- and one transition metal catalysts.

To begin with, we present an overview of different types of weak interactions, by using a set of prototypical binary complexes as shown in Fig. 1. Abundant literature on intermolecular interactions, both experimental and quantum chemical investigations, offer valuable insights on the nature of such weak interactions and their quantitative estimates.¹ While readers can refer to original literature to learn more about the nature of below-mentioned interactions, herein we list only those noncovalent interactions, which are more pertinent to the examples presented in the latter half of this manuscript. As can be gleaned from the summary of noncovalent interactions shown in Fig. 1, many of these interactions generally involve the

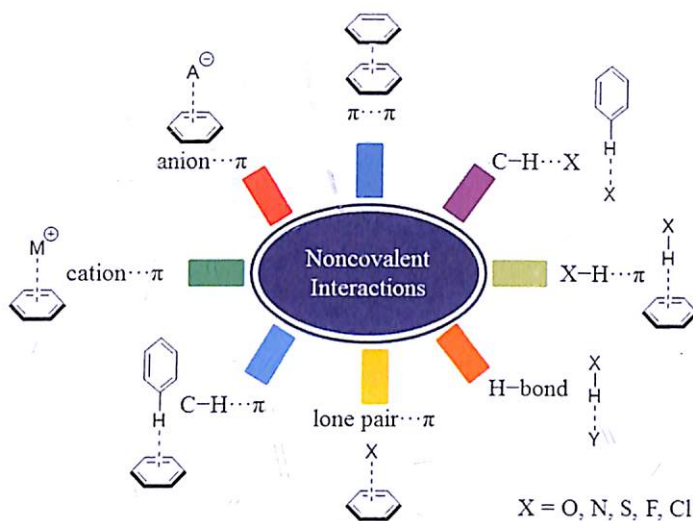


Fig. 1 General representation of different types of noncovalent interactions and the corresponding color codes used in this manuscript to depict such interactions in the stereocontrolling transition states.

participation of aryl or other unsaturated groups such as alkene/alkyne. The most common noncovalent interactions, including that found in the stereocontrolling transition states, are $\pi \cdots \pi$, $X-H \cdots \pi$, H-bond and ion $\cdots \pi$ interactions.² Each interaction is represented using a color code, which in turn, is used in the rest of the manuscript to help convey the presence of such interactions in a simpler way even in complicated transition state geometries.

Pioneering work by Dougherty shed light on cation $\cdots \pi$ interactions as an important interaction in both biological and chemical system.³ The stabilization rendered through various kinds of cation $\cdots \pi$ interaction is known to be important in determining protein structure and enzyme catalysis.⁴ Enhancement of binding energies by 2–5 kcal/mol due to cation $\cdots \pi$ interactions has been reported.⁵ Even stronger interactions are possible, such as when K^+ interacts with benzene, where the binding energy is as high as -19 kcal/mol in the gas phase.⁶ In simple terms, the cation $\cdots \pi$ interaction is attributed to a strong electrostatic interaction between the cation and electron cloud of the receptor, such as an aromatic ring or a double bond. Different studies indicate that the main stabilizing factor in cation $\cdots \pi$ complexes is an electrostatic interaction with significant contribution arising from dispersion as well as polarization.⁷

Anion $\cdots \pi$ interactions are another type of noncovalent force between an electron deficient aromatic system and anions.⁸ Earlier studies have provided structural evidence for anion $\cdots \pi$ interactions.⁹ The interaction energies due to the anion $\cdots \pi$ interactions could be in the range of 5–10 kcal/mol.¹⁰

The electrostatic and induction energies are the major contributors in this type of interaction wherein charge transfer from an anion to a π system is facilitated by inductive interaction between the HOMO of an anion and the LUMO of a π system. It also has a substantially greater contribution from the dispersion energies than that in cation $\cdots \pi$ interactions.¹¹ The role of dispersion is usually higher in case of organic anions, where the magnitude of dispersion can be even comparable to electrostatic and induction energies.¹²

A widely found interaction in biological systems are $\pi \cdots \pi$ interactions that are known to influence the structure of macromolecules.¹² Similar interactions are noticed in crystal structures of several organic and inorganic compounds. Theoretical studies on $\pi \cdots \pi$ interaction were generally carried out using benzene dimer as the prototypical example.¹³ Different geometry of interaction such as face-to-face, displaced face-to-face and edge-to-face structures was compared. Typical interaction energies in the T-shaped and parallel-displaced configurations are about -2.7 kcal/mol.¹⁴ The interaction energy in $\pi \cdots \pi$ complexes is dominated by dispersion interaction with a much smaller contribution from polarization.¹⁵

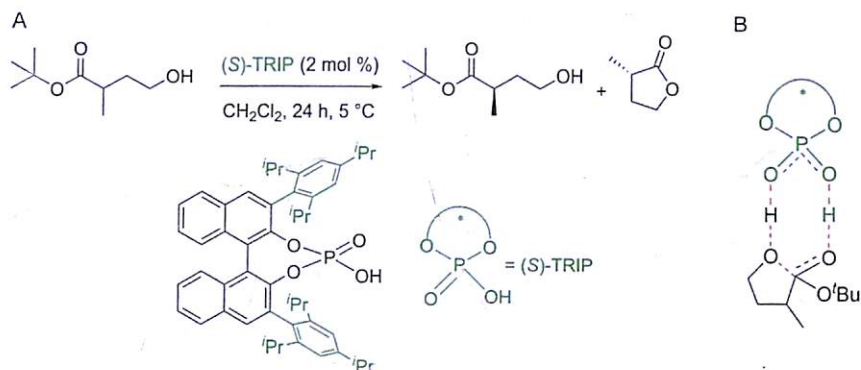
The $X-H \cdots \pi$ interactions (where $X=C, O, N$, halogen) are usually weaker than the ion $\cdots \pi$ interactions but a combination of several $X-H \cdots \pi$ interactions can make substantive contributions.¹⁶ The $X-H \cdots \pi$ is a type of hydrogen bonding interaction with a greater electrostatic component. Interestingly, dispersion energy becomes crucial in the case of $C-H \cdots \pi$ interaction involving sp^2 or sp^3 $C-H$ donors. Perhaps the very nature of $C-H \cdots \pi$ interaction, with both electrostatic and dispersion terms, makes it a ubiquitous weak interaction in chemical and biological systems. With an aromatic or aliphatic $C-H$ group as the H-donor and an aromatic ring as the acceptor, the calculated energy is in the range of $1.5-2.5$ kcal/mol.^{16a,17} The interactions involving aromatic $C-H$ are stronger than that of an unactivated aliphatic $C-H$ donor. For acidic CH groups (e.g., acetylene or chloroform) the interaction energy can increase to about $3-5$ kcal/mol, closer to that for conventional hydrogen bonds.^{16a} An important variant of $C-H \cdots \pi$ between an aromatic $C-H$ and an aromatic π system is of particular significance to the examples of asymmetric catalysis presented in this article.

Another weak interaction that is of immediate importance in asymmetric catalysis is hydrogen bonding. Hydrogen bonds also play significant roles in protein folding, protein-nucleic acid recognition, and other biological processes.¹⁸ There have been many experimental and theoretical studies aimed at studying H-bonded interactions in gaseous, liquid, and solid states.¹⁹ On the basis of criteria such as H-bond strength, geometrical and spectral

characteristics, H-bond interactions are classified as strong, moderate and weak.²⁰ The strength of these noncovalent interactions can vary all the way from 1 to 40 kcal/mol, with the classical H-bond strength falling in the window of 4–15 kcal/mol. The H-bonds are mainly governed by electrostatics albeit in some complexes charge transfer as well as partial covalent character is likely.²¹ In certain systems, dispersion with a moderate contribution from a polarization component is also reported as an important contributor.¹⁴ The electrostatic character of H-bond is mainly dominant in N–H...O, O–H...O, O–H...N bonds. The weaker H-bonds are defined as interactions where one or both the atoms are of low electronegativity.²² Some of the examples are C–H...O, C–H...N, C–H...O, C–H...F, C–H...Cl, etc.²³

The key questions are whether or not the above-mentioned weak interactions manifest themselves in a stereocontrolling transition state and how such forces could influence the relative energies of transition states. An accompanying complication with asymmetric catalysis is that the catalysts are larger than typical model systems shown in Scheme 1, making it increasingly harder to afford very high level of computations. Furthermore, several such interactions that coexist in the stereocontrolling transition states are intramolecular interactions, thus eluding direct quantification. In a stereocontrolling transition state, substrates that form the bond are covalently or noncovalently bound to the catalyst, thus any standard method of quantification of weak interactions using a super-system approach is a non-trivial exercise.²⁴ The interaction energy in an **A**...**B** super-system can be evaluated by comparing the energy of **A**...**B** (E_{AB}) with the sum of energies of the individual partners (E_A and E_B). Additional refinements to intermolecular interaction energies could be carried out by ameliorating potential impact of basis set superposition error arising due to the use of truncated basis sets as well as different number of basis functions that describes each interacting partner.^{15,25} Extension of such refinements would demand careful partitioning of the transition state structure into smaller fragments. Under such circumstances, alternative ways of analyzing intramolecular interactions in the transition states are required.

There have been several reports attempting to correlate interatomic contact distances, particularly between those atoms/groups which are lesser than the sum of van der Waals radii, as a measure of efficiency of weak interaction.²⁶ In recent years, different topological analysis of electron density took the center stage, wherein intramolecular interactions are analyzed by using Bader's atoms in molecules (AIM)²⁷ formalism or other reduced density



Scheme 2 (A) Enantioselective lactonization of hydroxy esters catalyzed by chiral phosphoric acid and (B) the corresponding the stereocontrolling transition state involving an intramolecular addition of the hydroxy group to the ester.

method such as the noncovalent interaction plots (NCI) formulated by Wang.²⁸ These protocols provide a relatively convenient way of identifying and conveying the presence of an otherwise complicated set of intramolecular interactions. For instance, the stereocontrolling transition states for an asymmetric lactonization reaction identified as the intramolecular addition of the hydroxyl group to the ester end of the molecule is shown in Scheme 2.²⁹ The examination of the green leaf-like patches in the NCI plot (Fig. 2A) conveys the presence of a region of attractive interactions.

The difference in noncovalent interactions between TS-*R* and TS-*S* is not conspicuous from the NCI plots. The bond paths that capture interatomic interactions can be used as a complementary tool to analyze the type of noncovalent interactions besides helping to delve further into the strength of such interactions. Although quantitative evaluation of the strength of individual interactions is not readily possible, one can develop an approximate idea of the relative strengths between a given type of interaction in the complex. For instance, there are two C–H⋯ π interactions in TS-*S* and two in TS-*R* (Fig. 2B). The question is whether two such interactions are more effective than another two such interactions that they help render improved stabilization to TS-*S*. Since the electron density at the bond critical point (ρ_{bcp}) can be considered as a measure of how effective a given interaction is, sum of electron densities might as well be an approximate way of quantifying the total interaction. This analysis suggests that overall TS-*S* exhibits better noncovalent interactions than TS-*R*.

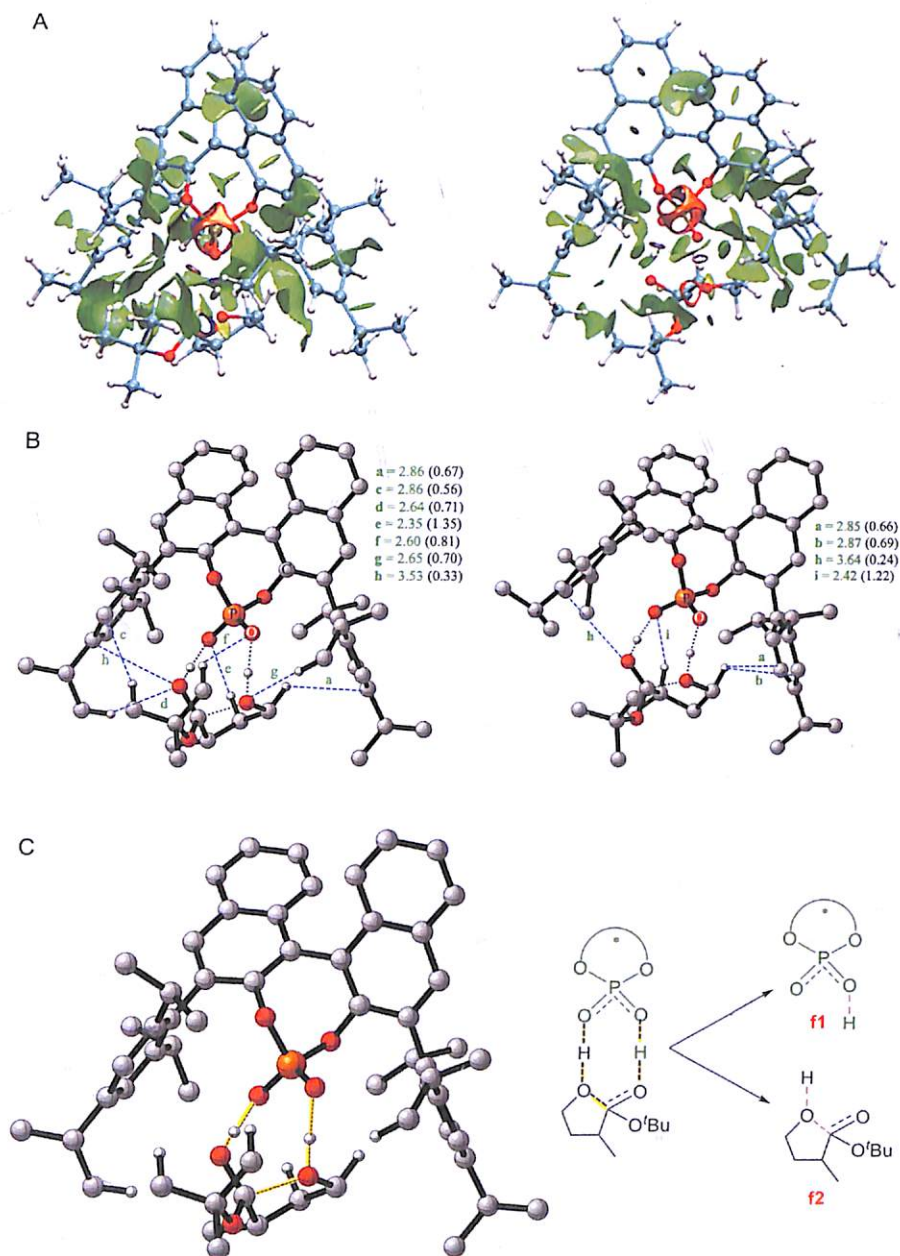


Fig. 2 (A) NCI plot and (B) bond critical points obtained through AIM analysis for stereocontrolling transition states (C) fragments of TS taken for activation strain analysis.

Another valuable tool for analyzing the origin of energy difference between the most preferred and less preferred stereochemical modes of reaction between the nucleophilic and electrophilic partners is activation strain/distortion interaction analysis.³⁰ The stereocontrolling transition state is

suitably partitioned into subunits, typically without impacting the region of the major bond formation (along the reaction coordinate shown in yellow highlight in Fig. 2C) and the interaction energy between such subunits are calculated. The distortions in each such subunit as noted in the transition state geometry is computed with respect to an undistorted ground state or the preceding intermediate. In the analysis of stereocontrolling transition states, the central question is on the relative interaction and distortion energies of TS-R with respect to that in TS-S.

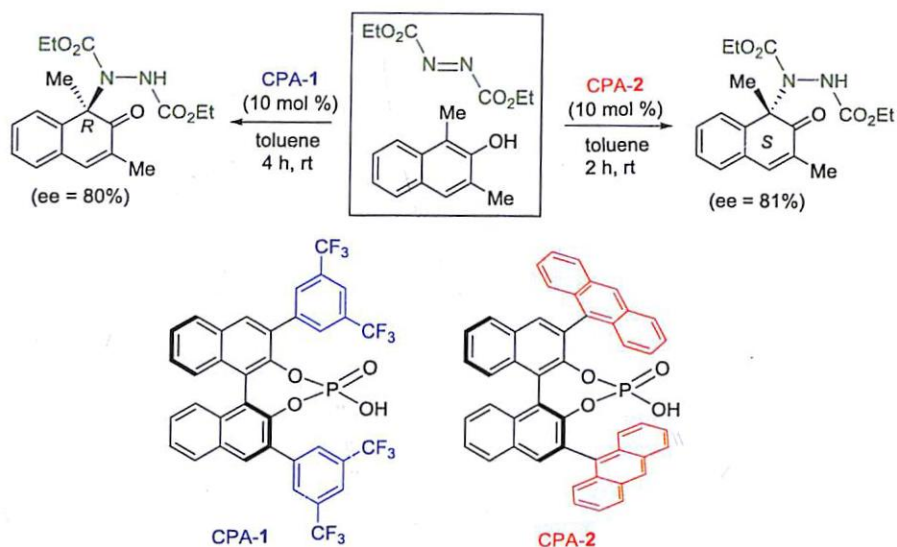
In the example shown in Scheme 2, in the lower energy TS-S the destabilization caused by distortion is lower compared to the corresponding values in TS-R. On the other hand, the stabilization due to interaction energy is more in the higher energy TS. The overall balance between the interaction and distortion energies was found to be in favor of the lower energy TS-S. This sort of analysis is simpler to carry out and the information that it provides could be exploited toward making informed alterations to the catalyst and/or the reactants for fine-tuning the enantioselectivity.

Thus far, we have presented a set of representative examples involving one catalyst that catalyzes the bond formation between two reactants. The following sections feature more interesting examples that employ more than two catalysts in one-pot reaction conditions. It is our intent to focus on the factors governing the stereoselectivity rather than a labyrinth of associated mechanistic details. Readers are encouraged to refer to the original literature for an in-depth discussion of various mechanistic steps in the catalytic cycle.



2. Asymmetric dearomative amination of β -naphthols

Asymmetric catalysis using chiral phosphoric acid (CPA) has emerged as a powerful tool in the recent years.³¹ One of the quintessential examples of this family of Brønsted acid catalysts are the chiral diols derived phosphoric acids, such as BINOL-phosphoric acid. These catalysts offer an effective Brønsted acidic and a moderately basic site capable of simultaneous activation of electrophilic and the nucleophilic reacting partners.³² The axial chirality along the binaphthyl rings is the source of chirality in CPA. The substituents at the 3,3' positions of the catalyst backbone are known to play a crucial role in determining the stereoselectivity of reactions.³³ The various noncovalent interactions between the substrate and 3,3' substituents can be harnessed for enhanced enantiocontrol.³⁴ The reversal of enantioselectivity for the same reaction could also be accomplished by varying the nature of substituents at



Scheme 3 Chiral BINOL-phosphoric acid catalyzed asymmetric dearomative amination of β -naphthols.

the 3,3' positions. In an interesting asymmetric dearomative amination of naphthols, as shown in Scheme 3, an inversion of enantioselectivity was demonstrated by changing the 3,3' substituent from 3,5-(CF₃)₂-C₆H₃ to 9-anthryl group.³⁵ In our recent study, we examined the mechanism and the enantiocontrolling transition states of this dearomatic amination reaction.³⁶ The stereocontrolling C–N bond formation transition states were located to gain insights into the origin of enantioselectivity.

The optimized geometries of the enantiocontrolling C–N bond formation TSs for CPA-1 and CPA-2 is shown in Fig. 3. With CPA-1 as the catalyst, the lower energy transition state was found to involve the addition of the *re* face of the α -methyl- β -naphthol to the *anti-anti* conformer of diethyl azodicarboxylate (DEAD) leading to the *R* enantiomer of the product. The most preferred transition state for the C–N bond formation through the *re* prochiral face was 1.7 kcal/mol lower in energy than the corresponding diastereomeric transition state for the *si* face addition. The lower energy TS enjoys a number of noncovalent interactions such as C–H \cdots F, C–H \cdots O, C–H \cdots π , lone pair \cdots π (Fig. 3). With CPA-2 as the catalyst, the preferred mode of addition is found to be the *si* face of the β -naphthol leading to the *S* enantiomer. The energy difference between these diastereomeric TSs was found to be 1.2 kcal/mol, which corresponds to a %ee of 76, in concert with the experimental value of 81. In the lower energy TS, more effective

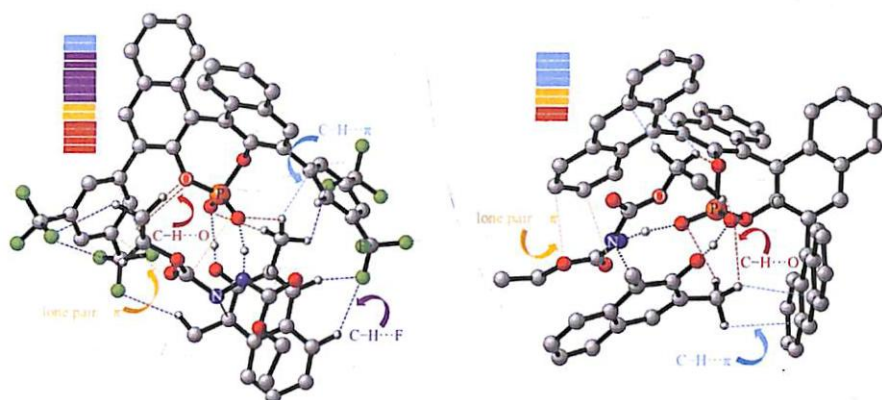
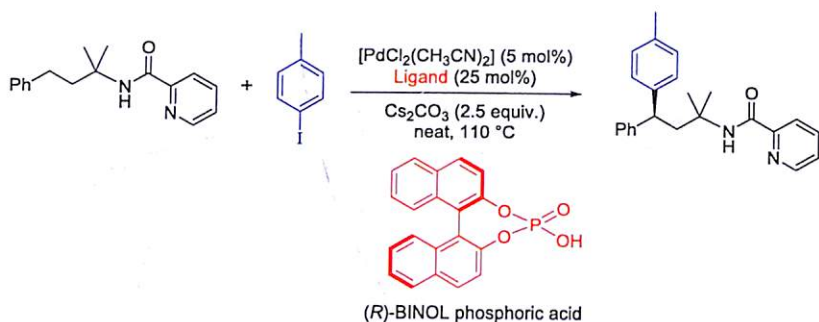


Fig. 3 Optimized geometries of the stereocontrolling C–N bond formation transition states for CPA-1 and CPA-2 as catalysts. Only selected hydrogen atoms are shown for improved clarity. Stacked colored blocks are provided for an easier comparison of the number of types of NCIs.

C–H \cdots O and C–H \cdots π interactions were noted as shown in Fig. 3. The inversion of enantioselectivity upon changing the 3,3' substituent from 3,5-(CF₃)₂-C₆H₃ (CPA-1) to 9-anthryl (CPA-2) was also investigated. In CPA-1, the dominant interaction is C–H \cdots F between –CF₃ of the catalyst and the C–H bonds of the β -naphthols and the ethyl group of DEAD. On the other hand, the noncovalent interactions in CPA-2 were dominated by the C–H \cdots π interaction with the anthryl arms of the catalyst, which leads to the change in preferred prochiral face for the C–N bond formation. These molecular insights clearly underscore how changes in the pattern of weak interaction could even result in inversion of enantioselectivity.

3. Pd-Catalyzed C–H Arylation

There have been good number of the interesting examples in the recent years on transition metal catalyzed C(sp³)–H bond activation reactions.³⁷ The use of chiral BINOL phosphoric acid derivatives in Pd-catalyzed enantioselective C–H bond reactions is of particular interest to the theme of this article.³⁸ As an illustration of this rapidly emerging form of asymmetric catalysis, here we wish to highlight a Pd-catalyzed benzylic C–H arylation using picolinamide as the directing group and (*R*)-BINOL phosphoric acid as a co-catalyst (Scheme 4).³⁹ Houk and co-workers have employed DFT (B3LYP/6-31G*, LANL2DZ + f(Pd)) computations to examine how chiral phosphate ligand controls the stereoselectivity of this arylation reaction.⁴⁰



Scheme 4 Pd-catalyzed C–H arylation directed by picolinamide in the presence of BINOL-phosphoric acid catalyst.

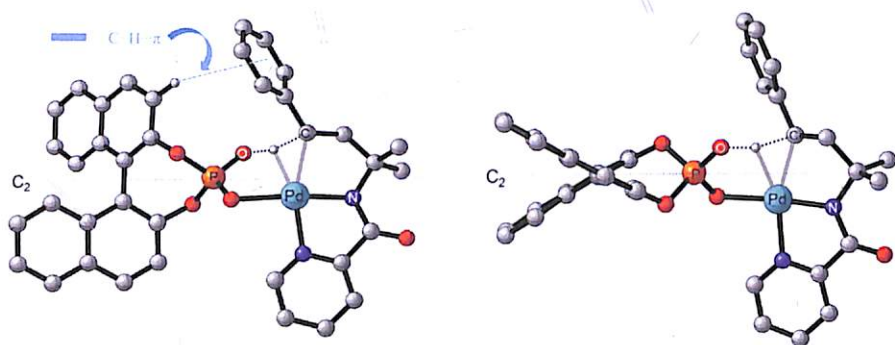


Fig. 4 Optimized geometries of two lower diastereomeric transition states.

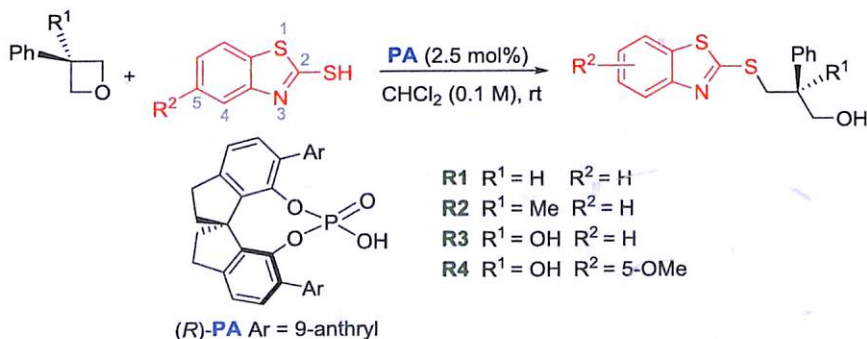
Detailed mechanistic investigation revealed that the C–H activation is the rate as well as stereoselectivity determining step wherein the chiral phosphate is considered as bound to the Pd center. The energy difference between the stereocontrolling TSs was found to be 3.2 kcal/mol, in favor of the (*S*) enantiomer of the product. A T-shaped geometry between the phenyl ring of the substrate and the naphthyl of (*R*)-BINOL phosphate leads to an edge-to-face aryl-aryl and C–H \cdots π interaction, which was found to be responsible for the observed enantioselectivity (Fig. 4). In the higher energy TS geometry, the phosphate ligand was perpendicular to the square planar region of the Pd(II) complex. As a consequence, the aforementioned C–H \cdots π was absent. In contrast, the ligand was found to remain coplanar with the square planar Pd(II) complex in the lower energy TS that facilitates the C–H \cdots π interaction between the ligand and the substrate (Fig. 4). In addition, the lower energy TS has an edge-to-face aryl-aryl interaction, which is missing in the corresponding higher energy TS. Additional computations, without the phenyl ring on the substrate, diminished the energy difference between the two TSs to half a kcal/mol. On the basis of this, it was proposed that the interaction between the chiral phosphate and the substrate

amounts to 2.7 kcal/mol. These observations suggest that the weak noncovalent interaction between substrate and the catalyst plays a direct role in rendering enantioselectivity in this benzylic C–H arylation reaction.

4. Desymmetrization of three-substituted oxetanes

In the examples presented thus far, the role of certain vital noncovalent interactions in the stereocontrolling TSs has been highlighted. Often, the presence of a large number of such weak interactions in a TS make it rather difficult to attribute the origin of observed stereoselectivity to only one primary factor. Following is an example of an oxetane desymmetrization by using SPINOL derived phosphoric acid.⁴¹ The ring opening of three-substituted phenyloxetanes by mercaptobenzothiazole as the nucleophile can furnish products bearing a quaternary stereocenter (Scheme 5).⁴² Computational investigations by the Wheeler group provided valuable insights on the origin of stereoselectivity for four different substrate variations with *ees* ranging from 77 to >99.⁴³

The reaction is proposed to proceed through an S_N2-type mechanism wherein the addition of the nucleophile and the ring opening of oxetane were found to occur simultaneously. In the case of un/mono-substituted phenyloxetane, the energy difference between the two stereocontrolling TSs was found to be 1.6 kcal/mol which corresponds to 87% *ee*, and is in excellent agreement with the experimental value of 88%. The interaction energy (as obtained using the distortion–interaction analysis) between the substrate and the catalyst was found to be primarily responsible for the stereoselectivity. More efficient C–H⋯ π interaction led to enhanced stabilization of the lower energy TS (Fig. 5). A reduction in the extent of stereoselectivity (*%ee* = 77) was noted upon inclusion of a methyl substituent



Scheme 5 Desymmetrization of three-substituted oxetanes catalyzed by phosphoric acid.

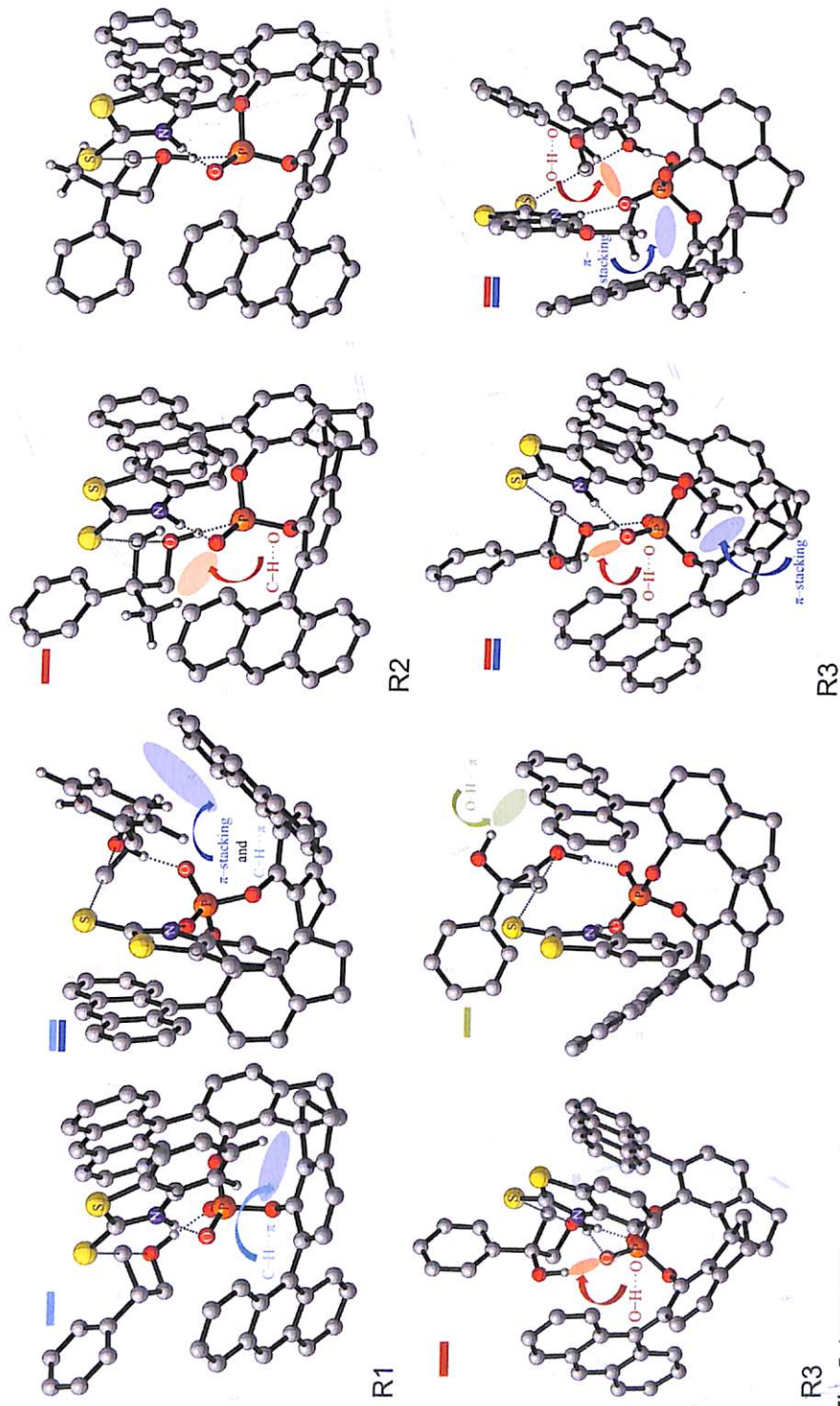


Fig. 5 Important noncovalent interactions in different substrate variations. Stacked colored blocks are provided for an easier comparison of the number of types of NCIs.

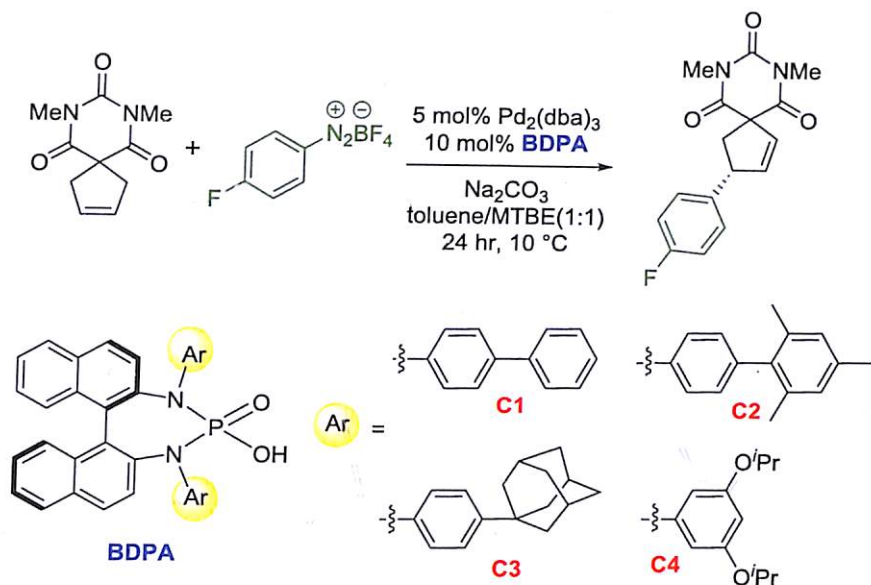
at the 3rd position of the phenyl oxetane (**R2**). Whereas the C–H $\cdots\pi$ interaction played a critical role in determining the enantioselectivity of the unsubstituted phenyl oxetanes **R1**, the C–H \cdots O interaction between methyl substituent and phosphoric acid was found to be more important in the case of 3-methyl phenyl oxetane **R2** (Fig. 5).

Improved enantioselectivity of 97% was noticed when a –OH group (**R3**) is introduced at the 3-position of phenyl oxetane. The O–H \cdots O hydrogen bonding interaction between the –OH group of the phenyl oxetane and the phosphate oxygen was found to provide additional stabilization to the lower energy TS by 4.3 kcal/mol (computed %*ee* = > 99). A further improvement in enantioselectivity was reported upon substituting the 5-position of mercaptobenzothiazole with an –OMe group (**R4**) (experimental and computed %*ee* = > 99). Relatively larger distortion of the catalyst was noted in the TS with substrate **R4**. Among the noncovalent interactions, the more favorable O–H \cdots O interaction between the –OH group of phenyl oxetane and the catalyst as well as the π -stacking between the nucleophile and catalyst was found to be more prominent in the lower energy TS (Fig. 5).

From the above examples it is clear that the mode of stereoinduction changes even with a small variation in the structure of the catalyst, making it difficult to give a generalizable stereochemical model.

5. Enantioselective heck matsuda arylation

The asymmetric synthesis of complex targets has been successfully achieved using transition metal catalyzed cross-coupling reactions.⁴⁴ As a typical variant of coupling reactions, we present an interesting Heck–Matsuda reaction as shown in Scheme 6. In this dual catalytic reaction, Pd₂(dba)₃ is used as a transition metal catalyst in conjunction and a BINAM derived phosphoric acid as an organocatalyst, for the arylation of olefins by aryl diazonium salts.⁴⁵ This example assumes additional significance owing to the scarcity of asymmetric variants of Heck–Matsuda coupling.⁴⁶ Recently, an enantioselective Heck–Matsuda coupling was reported under chiral anion phase transfer conditions using aryl diazonium salts with BDPA catalyst bearing Ar = 4-adamantyl–C₆H₄.⁴⁷ Another fascinating example of the enantioselective Heck–Matsuda arylation of spirocyclic cyclopentene with 4-fluorophenyldiazonium tetrafluoroborate using a catalytic dyad consisting of Pd₂(dba)₃ and BINAM derived phosphoric acid is shown in Scheme 6. We investigated the mechanism and the origin of stereoselectivity with a goal of predicting the enantioselectivity with catalysts/substrate variations that were not reported earlier.⁴⁸



Scheme 6 A dual-catalytic enantioselective Heck-Matsuda arylation of spirocyclic pentene with $\text{Pd}_2(\text{dba})_3$ and BDPA catalyst.

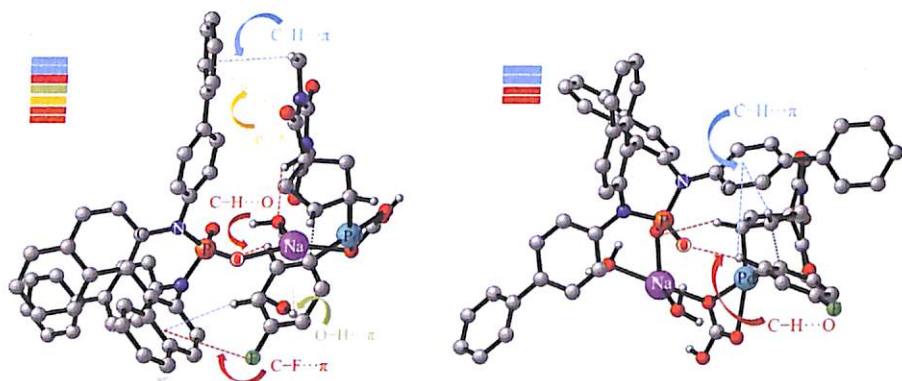
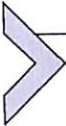


Fig. 6 Noncovalent interactions observed in the two lower energy diastereomeric migratory insertion TSs. Stacked colored blocks are provided for an easier comparison of the number of types of NCIs.

A detailed computational investigation was undertaken first to learn that the migratory insertion of the Pd-bound aryl group to the alkenyl moiety in the Pd-aryl intermediate (formed through the oxidative insertion of Pd(0) on the diazonium salt) is the enantiocontrolling step. The aryl group migration to the *si* face of the spirocyclic alkene giving the *R* enantiomer of the product was found to be marginally preferred over that to the *re* face. The Gibbs free energy difference between the two diastereomeric TSs was found to be 0.5 kcal/mol , which corresponds to *%ee* of 39. The lower energy TS is dominated by various noncovalent interactions such as $\text{O-H}\cdots\pi$, $\text{C-H}\cdots\text{O}$, $\text{C-H}\cdots\pi$, lone pair $\cdots\pi$, and $\text{C-F}\cdots\pi$ (Fig. 6).

On the basis of the molecular insights gathered from one and only one experimentally known example of a low *ee* of 34%, the authors set out to perform a series of modifications and predicted how the %*ee* would vary. These modifications were aimed at changes to the nature of the N-aryl substituents as those interacted with the substrate and exhibited differential interaction between the *re* and *si* face migration. Computations on three newly modified catalysts (**C2**, **C3**, **C4**) keeping the substrate combination same (Scheme 6) showed a modulation in the *ee*. By changing the 4-aryl substituent of N-aryl group to diisopropoxy (**C4**), mesityl (**C2**) and adamantyl (**C3**), a greater number of effective noncovalent interactions were seen in the stereocontrolling TSs leading to an increase in the computed %*ee* to 89. A number of experiments were subsequently performed based on the computational predictions and good agreements were observed.

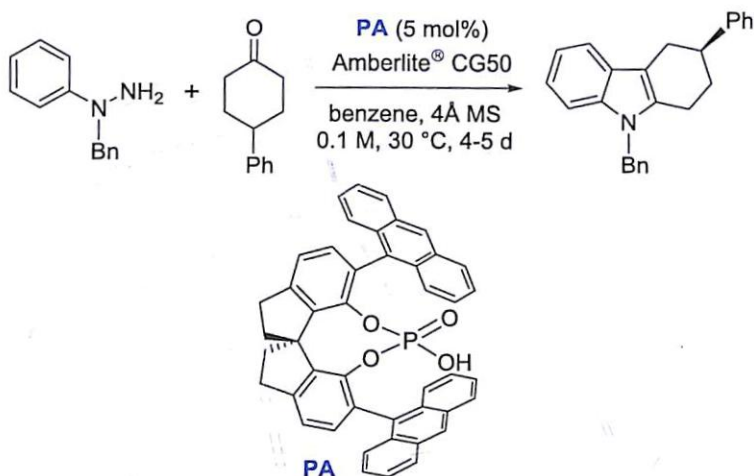
The example described above is an interesting demonstration of how the knowledge of noncovalent interactions in the stereocontrolling transition states could be harnessed in asymmetric catalysis and help in the design of new chiral catalysts or ligands.



6. Enantioselective synthesis of indoles

In nature the indole ring is seen as one of the most ubiquitous heterocycle and therefore an important component in pharmaceuticals.⁴⁹ The Fischer indole synthesis is an important reaction to obtain indoles from phenylhydrazine and an aldehyde or ketone under acidic conditions.⁵⁰ The mechanism involves the formation of phenylhydrazone followed by rearrangement to ene-hydrazine. After protonation of the phenyl nitrogen, a [3,3]-sigmatropic rearrangement gives an imine. The next step includes the formation of a cyclic aminal, and eliminating NH₃ leads to the favorable aromatic indole. Scheme 7 shows SPINOL-phosphoric acid catalyzed enantioselective synthesis of indoles.⁵¹ Wheeler and co-workers have studied the enantioselective step of the reaction to quantify the role of noncovalent interactions.⁵²

Authors found that the [3,3]-sigmatropic rearrangement was the stereoselective step. The TS leading to the (*R*) enantiomer of the product was found to be 2.7 kcal/mol higher in energy than that corresponds to the (*S*) enantiomer. In the lower energy TS, two N–H···O hydrogen bonding interactions between the protonated substrate and the catalyst were found as compared to only one such interaction in the higher energy TS (Fig. 7). The π stacking interactions between the substrate and anthracenyl group were found



Scheme 7 Enantioselective synthesis of indoles catalyzed by SPINOL derived phosphoric acid.

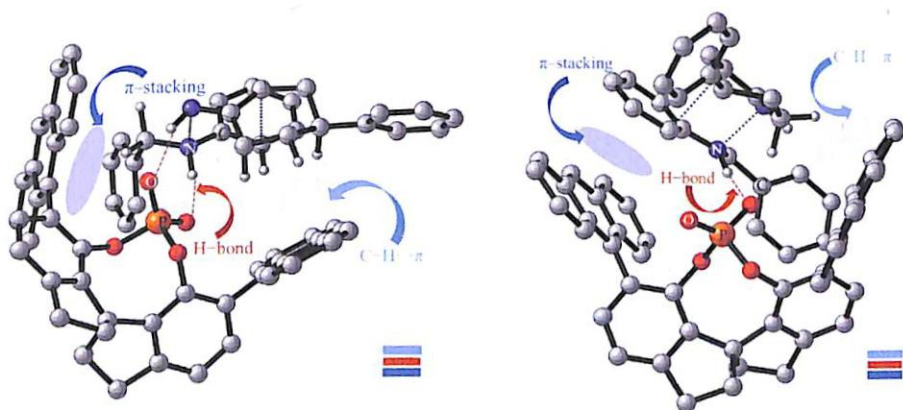
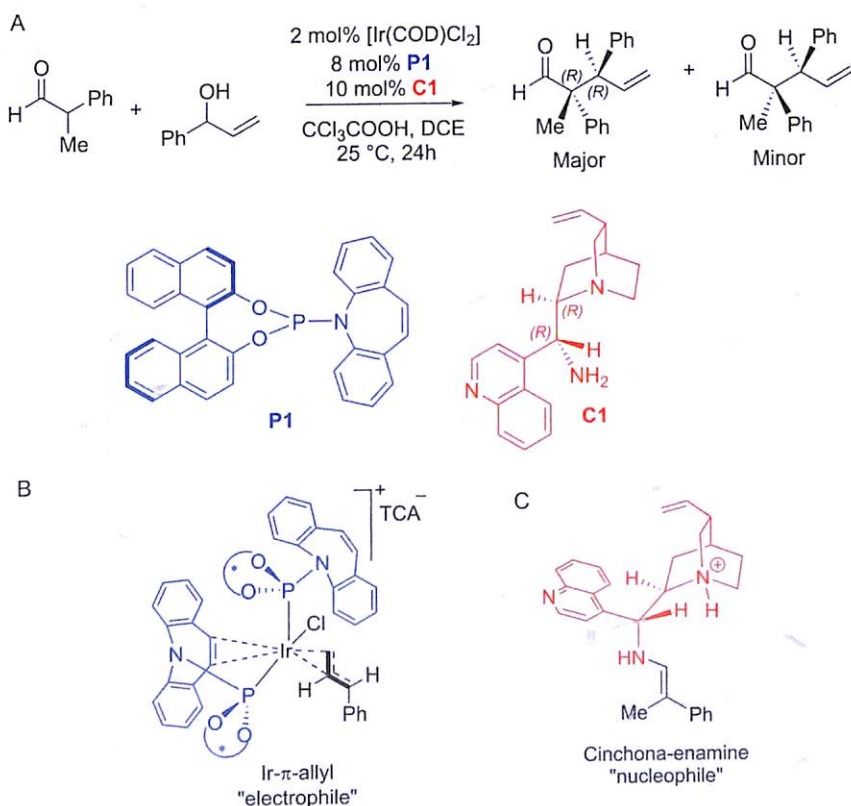


Fig. 7 The stereocontrolling [3,3]-sigmatropic rearrangement transition states showing the important noncovalent interactions. Stacked colored blocks are provided for an easier comparison of the number of types of NCIs.

to provide preferential stabilization to the higher energy TS. Furthermore, the lower energy TS exhibited C–H... π interactions between (a) the cyclohexenyl and the anthracenyl groups and (b) aromatic C–H bonds of the phenyl of the phenylhydrazine and the anthracenyl group (Fig. 7). These C–H... π interactions in the lower energy TS more than compensates for the favorable π stacking interactions noted in the higher energy TS. The substrate could not fit well into the binding pocket of the chiral catalyst due to lack of these favorable C–H... π interactions while maintaining the π stacking interactions in the case of the higher energy TS.

7. Asymmetric α -allylation of aldehydes

The preceding examples in this article described how the noncovalent interactions influence the stereoselectivity in a select set of transition metal catalysis controlled by a chiral ligand⁵³ or organocatalysts interacting with the substrate by various noncovalent interactions.⁵⁴ An obvious extension of these two independent and well-developed forms of catalysis is to examine the implications when two chiral catalysts are engaged in the same reaction under one-pot conditions. Here, the cooperative catalysis comes into picture where the electrophile and the nucleophile are separately activated by two catalysts.⁵⁵ Many interesting examples of cooperative catalysis can also be found in Nature.⁵⁶ One such example of asymmetric dual catalysis employing a combination of organo- and transition metal catalysis is shown in Scheme 8A.⁵⁷ In our recent efforts, we investigated the mechanism and the origin of stereodivergence in this dual catalytic reaction.⁵⁸



Scheme 8 (A) Asymmetric α -allylation of an aldehyde employing phosphoramidite and cinchona dual chiral catalysts, (B) Ir- π -allyl complex, and (C) cinchona-enamine complex.

The reactants include an aldehyde and an allyl alcohol. The chiral cinchona catalyst activates the aldehyde by forming an enamine (Scheme 8C). The allyl alcohol is activated by the trifluoroacetic acid in the presence of a chiral iridium-phosphoramidite catalyst to give Ir- π -allyl complex (Scheme 8B). Both the activated substrates can now participate in C–C bond formation through their prochiral faces to give two chiral carbon centers. The C–C bond formation TS between the prochiral faces of nucleophile and electrophile can lead to four product stereoisomers that differ in their configurations. For instance, the combination of (*R*)-phosphoramidite and (*R,R*)-cinchona leads to the (*2R,3R*) product. An inversion in configuration at the α stereocenter was observed by using (*S,S*)-cinchona. On the other hand, the stereocenter at the β carbon could be inverted by using (*S*)-phosphoramidite. To gain insights into the origin of stereodivergence for different catalyst combinations, the stereocontrolling C–C bond formation TSs were located.

The optimized geometries of C–C bond formation TSs for the catalyst combination (*R,R*)-cinchona and (*R*)-phosphoramidite are given in Fig. 8. The lower energy TS involves the addition of the *re* face of cinchona enamine to the *si* face of Ir- π -allyl intermediate, leading to (*2R,3R*) product. The TSs with *si-si* and *si-re* modes of addition was respectively found to be 3.3 and 7.6 kcal/mol higher than the *re-si* mode of addition. This indicates high enantio- and diastereoselectivity, which was the case with the experimental observation. As with the previous examples presented in this compilation, a good number of weak noncovalent interactions such as C–H $\cdots\pi$, $\pi\cdots\pi$, lone pair $\cdots\pi$, N \cdots H, Cl \cdots H were identified in the lower energy TS. Among these the most critical ones are (a) π stacking interactions between the quinoline arm of cinchona and the phenyl ring of allylic substrate, (b) C–H $\cdots\pi$ interactions between the azepine olefinic C–H and the phenyl ring of the enamine. These interactions were found to be lesser in number and weaker in strength in the higher energy TS. In addition, in the higher energy TSs the disposition of the quinoline arm of cinchona was not suitable to afford a π stacking interaction.

From all the examples presented in this article, we can conclude that the knowledge of noncovalent interactions in the stereocontrolling TSs can help in improving the scope and efficiency of asymmetric transformations. The cumulative impact of a series of noncovalent interactions can become a critical control element in asymmetric catalysis. Hence, the analysis of such weak interactions in the stereocontrolling transition states as described earlier in the earlier sections, gains additional significance. The way forward evidently encourages one a rethink on qualitative steric-only transition state models.

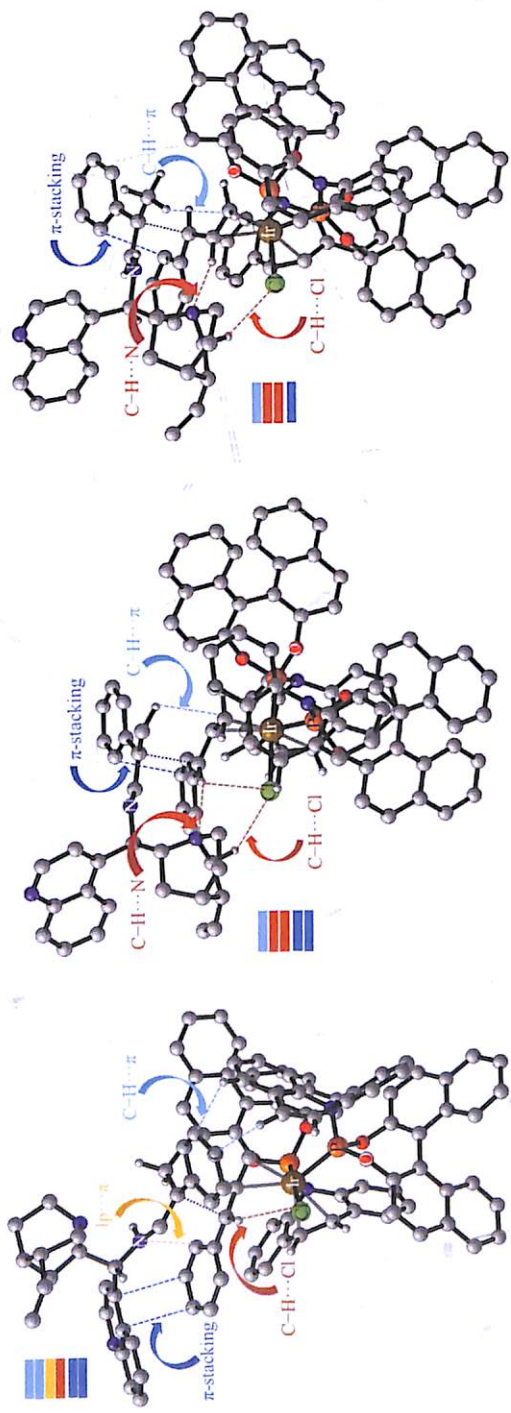


Fig. 8 Optimized geometries of stereocontrolling C–C bond formation TSs showing various noncovalent interactions. Stacked colored blocks are provided for an easier comparison of the number of types of NCIs.



8. Summary and outlook

Steady improvements in computing technology, ably complemented by the availability of more efficient versions of density functional methods, have made computational studies increasingly more amenable on larger molecular systems. In the domain of asymmetric catalysis, these benefits are expressed in the form of our ability to derive valuable insights on the energetics of catalytic transformations, access to geometric and electronic details of various intermediates and transition states. Most important of all such computations in asymmetric catalysis is about the stereocontrolling transition states. One can decipher the presence of weak noncovalent interactions and learn how they exert a vital influence in determining the relative energies of transition states responsible for the formation of different enantiomers. Molecular level understanding of such transition state could be exploited as a rational framework toward modifying the existing catalyst and also in the choice of suitable substrates in the development of asymmetric catalysis. While the traditional use of computational tools for rationalizing experimental observations continues to address complex reaction mechanism problems, the current trends also indicate the power of such methods in guiding development of new experiments. We believe that in the near future we would witness more activities in this front where computational predictions could go hand in hand with experimental discovery of asymmetric catalysts, and perhaps even afford predictions for tangible experimental verification.

References

1. (a) Gallivan JP, Dougherty DA. Cation- π interactions in structural biology. *Proc Natl Acad Sci USA*. 1999;96:9459–9464. (b) Moore III KB, Sadeghian K, Sherrill CD, Ochsenfeld C, Schaefer III HF. C–H \cdots O hydrogen bonding. The prototypical methane–formaldehyde system: a critical assessment. *J Chem Theory Comput*. 2017;13:5379–5395. (c) Tewari AK, Srivastava P, Singh VP, et al. Selective induced polarization through electron transfer in acetone and pyrazole ester derivatives via C–H \cdots O=C interaction. *New J Chem*. 2014;38:4885–4892. (d) Kolar MH, Carloni P, Hobza P. Statistical analysis of σ -holes: a novel complementary view on halogen bonding. *Phys Chem Chem Phys*. 2014;16:19111–19114. (e) Rezac J, Nachtigalova D, Mazzoni F, et al. Binding energies of the π -stacked anisole dimer: new molecular beam–laser spectroscopy experiments and CCSD(T) calculations. *Chem A Eur J*. 2015;21:6740–6746. (f) Mahadevi AS, Sastry GN. Cooperativity in noncovalent interactions. *Chem Rev*. 2016;116:2775–2825.
2. (a) Salonen LM, Ellermann M, Diederich F. Aromatic rings in chemical and biological recognition: energetics and structures. *Angew Chem Int Ed*. 2011;50:4808–4842. (b) Martin N, Nierengarten JF. *Supramolecular Chemistry of Fullerenes and Carbon*

- Nanotubes*. Weinheim, Germany: Wiley-VCH Verlag & Co. KGaA; 2012. (c) Perez EM, Martín N. $\pi\cdots\pi$ interactions in carbon nanostructures. *Chem Soc Rev*. 2015;44:6425–6433. (d) Tsuzuki S, Uchimaru T. Magnitude and physical origin of intermolecular interactions of aromatic molecules: recent progress of computational studies. *Curr Org Chem*. 2006;10:745–762.
- Shepodd T, Petti MA, Dougherty DA. Molecular recognition in aqueous media: donor-acceptor and ion-dipole interactions produce tight binding for highly soluble guests. *J Am Chem Soc*. 1988;110:1983–1985.
 - Mahadevi AS, Sastry GN. Cation– π interaction: its role and relevance in chemistry, biology, and material science. *Chem Rev*. 2013;113:2100–2138.
 - (a) Scharer K, Morgenthaler M, Paulini R, et al. Quantification of cation– π interactions in protein-ligand complexes: crystal-structure analysis of factor Xa bound to a quaternary ammonium ion ligand. *Angew Chem Int Ed*. 2005;44:4400–4404. (b) Ting AY, Shin I, Lucero C, Schultz PG. Energetic analysis of an engineered cation– π interaction in staphylococcal nuclease. *J Am Chem Soc*. 1998;120:7135–7136.
 - Sunner J, Nishizawa K, Kerbarle P. Ion-solvent molecule interactions in the Gas-phase: the potassium-ion and benzene. *J Phys Chem*. 1981;85:1814.
 - (a) Dougherty DA. The cation– π interaction. *Acc Chem Res*. 2013;46:885–893. (b) Carrazana-García JA, Cabaleiro-Lago EM, RodríguezOtero J. A theoretical study of complexes formed between cations and curved aromatic systems: electrostatics does not always control cation– π interaction. *Phys Chem Chem Phys*. 2017;19:10543–10553. (c) Sherrill CD. Energy component analysis of π interactions. *Acc Chem Res*. 2013;46:1020–1028.
 - Quinonero D, Garau C, Rotger C, et al. Anion– π interactions: do they exist? *Angew Chem Int Ed Engl*. 2002;41:3389–3392.
 - Berryman OB, Johnson DW. Experimental evidence for interactions between anions and electron-deficient aromatic rings. *Chem Commun*. 2009;3143–3153.
 - (a) Mascall M, Armstrong A, Bartberger MT. Anion–aromatic bonding: a case for anion recognition by π -acidic rings. *J Am Chem Soc*. 2002;124:6274–6276. (b) Alkorta I, Rozas I, Elguero J. Interaction of anions with perfluoro aromatic compounds. *J Am Chem Soc*. 2002;124:8593–8598.
 - Kim D, Tarakeshwar P, Kim KS. Theoretical investigations of anion– π interactions: the role of anions and the nature of π systems. *J Phys Chem A*. 2004;108:1250–1258.
 - (a) Meyer EA, Castellano RK, Diederich F. Interactions with aromatic rings in chemical and biological recognition. *Angew Chem Int Ed*. 2003;42:1210–1250. (b) Cerny J, Kabelac M, Hobza P. Double-helical-ladder structural transition in the B-DNA is induced by a loss of dispersion energy. *J Am Chem Soc*. 2008;130:16055–16059.
 - (a) Lee EC, Hong BH, Lee JY, et al. Substituent effects on the edge-to-face aromatic interactions. *J Am Chem Soc*. 2005;127:4530–4537. (b) Sinnokrot MO, Sherrill CD. Substituent effects in π - π interactions: sandwich and T-shaped configurations. *J Am Chem Soc*. 2004;126:7690–7697.
 - (a) Podeszwa R, Bukowski R, Szalewicz K. Potential energy surface for the benzene dimer and perturbational analysis of π - π interactions. *J Phys Chem A*. 2006;110:10345–10354. (b) Sinnokrot MO, Valeev EF, Sherrill CD. Estimates of the ab initio limit for π - π interactions: the benzene dimer. *J Am Chem Soc*. 2002;124:10887–10893. (c) Lee EC, Kim D, Jurecka P, Tarakeshwar P, Hobza P, Kim KS. Understanding of assembly phenomena by aromatic-aromatic interactions: benzene dimer and the substituted systems. *J Phys Chem A*. 2007;111:3446–3457. (d) Kokkin D, Ivanov MV, Loman J, Cai JZ, Rathore R, Reid SA. Strength of π -stacking, from neutral to cation: precision measurement of binding energies in an isolated π -stacked dimer. *J Phys Chem Lett*. 2018;9:2058–2061. (e) Mazzoni F, Pasquini M, Pietraperzia G, Becucci M. Binding energy determination in a π -stacked aromatic

- cluster: the anisole dimer. *Phys Chem Chem Phys*. 2013;15:11268–11274. (f) Rezac J, Hobza P. Ab initio quantum mechanical description of noncovalent Interactions at its limits: approaching the experimental dissociation energy of the HF dimer. *J Chem Theory Comput*. 2014;10:3066–3073.
15. Sharma B, Srivastava HK, Gayatri G, Sastry GN. Energy decomposition analysis of cation- π , metal ion-lone pair, hydrogen bonded, charge-assisted hydrogen bonded, and π - π interactions. *J Comput Chem*. 2015;36:529–538.
 16. (a) Nishio M. The CH/ π hydrogen bond in chemistry. Conformation, supramolecules, optical resolution and interactions involving carbohydrates. *Phys Chem Chem Phys*. 2011;13:13873–13900. (b) Nishio M, Umezawa Y, Fantini J, Weiss MS, Chakrabarti P. CH- π hydrogen bonds in biological macromolecules. *Phys Chem Chem Phys*. 2014;16:12648–12683.
 17. (a) McKinnon JJ, Jayatilaka D, Spackman MA. Towards quantitative analysis of intermolecular interactions with Hirshfeld surfaces. *Chem Commun*. 2007;37:3814–3816. (b) Mohan N, Vijayalakshmi KP, Koga N, Suresh CH. Comparison of aromatic NH \cdots π , OH \cdots π , and CH \cdots π interactions of alanine using MP2, CCSD, and DFT methods. *J Comput Chem*. 2010;31:2874–2882. (c) Sherrill CD, Sumpter BG, Shinnokrot MO, et al. Assessment of standard force field models against High-quality ab initio potential curves for prototypes of pi- π , CH/pi, and SH/pi interactions. *J Comput Chem*. 2009;30:2187–2193. (d) Hunter A, Sanders JKM. The nature of pi-pi interactions. *J Am Chem Soc*. 1990;112:5525–5534. (e) Hunter CA. The role of aromatic interactions in molecular recognition. *Chem Soc Rev*. 1994;23:101–109.
 18. (a) Westhof E. Isostericity and tautomerism of base pairs in nucleic acids. *FEBS Lett*. 2014;588:2464–2469. (b) Li PTX, Viereggs J, Tinoco Jr I. How RNA unfolds and refolds. *Annu Rev Biochem*. 2008;77:77–100. (c) Dill KA, MacCallum JL. The protein-folding problem, 50 years on. *Science*. 2012;338:1042–1046. (d) Gromiha MM, Siebers JG, Selvaraj S, Kono H, Sarai A. Role of inter and intramolecular interactions in protein-DNA recognition. *Gene*. 2005;364:108–113.
 19. (a) Jeffrey GA. *An Introduction to Hydrogen Bonding*. New York: Oxford University Press; 1997. (b) Scheiner S. *Hydrogen Bonding. A Theoretical Perspective*. Oxford, UK: Oxford University Press; 1997.
 20. (a) Desiraju GR, Steiner T. *The Weak Hydrogen Bond in Structural Chemistry and Biology*. Oxford, UK: Oxford University Press; 1999. (b) Desiraju GR. Hydrogen bridges in crystal engineering: interactions without borders. *Acc Chem Res*. 2002;35:565–573.
 21. (a) Steiner T, Majerz I, Wilson CC. First O-H \cdots N hydrogen bond with a centered proton position obtained by thermally induced proton migration. *Angew Chem Int Ed Engl*. 2001;40:2651–2654. (b) Vishweshwar P, Nangia A, Lynch VM. Cooperative assistance in a very short O-H \cdots O hydrogen bond. Low-temperature X-ray crystal structures of 2,3,5,6-pyrazinetetracarboxylic and related acids. *Chem Commun*. 2001;179–180. (c) Wilson CC. Migration of the proton in the strong O-H \cdots O hydrogen bond in urea-phosphoric acid (1/1). *Acta Crystallogr B*. 2001;57:435–439.
 22. Desiraju GR, Steiner T. *The Weak Hydrogen Bond in Structural Chemistry and Biology*. Oxford: Oxford University Press; 1999.
 23. (a) Lee H, Knobler CB, Hawthorne MF. Supramolecular selfassembly directed by carborane C-H \cdots F interactions. *Chem Commun*. 2000;24:2485–2486. (b) Aullon G, Bellamy D, Brammer L, Bruton E, Orpen AG. Metal-bound chlorine often accepts hydrogen bonds. *Chem Commun*. 1998;653–654. <https://doi.org/10.1039/A709014E>. (c) Aakeroy CB, Evans TA, Seddon KR, Palinko I. The C-H \cdots Cl hydrogen bond: does it exist? *New J Chem*. 1999;23:145–152. (d) Moore III KB, Sadeghian K, Sherrill CD, Ochsenfeld C, Schaefer III HF. C-H \cdots O hydrogen bonding. The prototypical methane-formaldehyde system: a critical assessment. *J Chem Theory Comput*. 2017;13:5379–5395.

24. (a) A number of quantification schemes can be found in literature that employs second order perturbation theory as well as other ways of reformulating the intermolecular interactions by way of partitioning of the transition state to smaller fragments.; (b) Bakr BW, Sherrill CD. Analysis of transition state stabilization by non-covalent interactions in the Houk–list model of organocatalyzed intermolecular aldol additions using functional-group symmetry-adapted perturbation theory. *Phys Chem Chem Phys* 2016;18:10297–10308
25. Malakar S, Sowndarya SV, Sunoj RB. A quantification scheme for non-covalent interactions in the enantio-controlling transition states in asymmetric catalysis. *Org Biomol Chem*. 2018;16:5643–5652.
26. Roy D, Sunoj RB. Quantification of intramolecular nonbonding interactions in organo-chalcogens. *J Phys Chem A*. 2006;110:5942–5947.
27. (a) AIM2000 Version 2.0. *Buro fur Innovative Software*. Bielefeld, Germany: SBK-Software; 2002. (b) Bader RFW. A quantum theory of molecular structure and its applications. *Chem Rev*. 1991;91:893–928. (c) Biegler-Konig F, Schonbohm J, Bayles D. AIM2000 a program to analyze and visualize atoms in molecules. *J Comput Chem*. 2001;22:545–559.
28. (a) Johnson ER, Keinan S, Mori-Sánchez P, Contreras-García J, Cohen AJ, Yang W. Revealing noncovalent interactions. *J Am Chem Soc*. 2010;132:6498–6506. (b) Contreras-García J, Johnson ER, Keinan S, et al. NCIPLOT: a program for plotting non-covalent interaction regions. *J Chem Theory Comput*. 2011;7:625–632. For more examples on NCIs in catalysis see: (a) Sunoj RB. Transition state models for understanding the origin of chiral induction in asymmetric catalysis. *Acc Chem Res*. 49 (2016) 1019–1028; (b) Tribedi S, Hadad CM, Sunoj RB. Origin of stereoselectivity in the amination of alcohols using cooperative asymmetric dual catalysis involving chiral counterion. *Chem Sci*. 9 (2018) 6126–6133. (c) Unnikrishnan A, Sunoj RB. Insights into the role of noncovalent interactions in distal functionalization of the aryl C(sp²)-H bond. *Chem Sci*. 2019;10:3826–3835.
29. Changotra A, Sunoj RB. Origin of kinetic resolution of hydroxy esters through catalytic enantioselective lactonization by chiral phosphoric acids. *Org Lett*. 2016;18:3730–3733.
30. Bickelhaupt FM, Houk KN. Analyzing reaction rates with the distortion/interaction-activation strain model. *Angew Chem Int Ed*. 2017;56:10070–10086.
31. Maji R, Mallojjala SC, Wheeler SE. Chiral phosphoric acid catalysis: from numbers to insights. *Chem Soc Rev*. 2018;47:1142–1158.
32. (a) Parmar D, Sugiono E, Raja S, Rueping M. Complete field guide to asymmetric BINOL-phosphate derived brønsted acid and metal catalysis: history and classification by mode of activation; brønsted acidity, hydrogen bonding, ion pairing, and metal phosphates. *Chem Rev*. 2014;114:9047–9153. (b) Reid JP, Simon L, Goodman JM. A practical guide for predicting the stereochemistry of bifunctional phosphoric acid catalyzed reactions of imines. *Acc Chem Res*. 2016;49:1029–1041.
33. Melikian M, Grammüller J, Hioe J, Greindl J, Gschwind RM. Brønsted acid catalysis—the effect of 3,3′-substituents on the structural space and the stabilization of imine/phosphoric acid complexes. *Chem Sci*. 2019;10:5226–5234. <https://doi.org/10.1039/c9sc01044k>.
34. (a) Reid JP, Goodman JM. Goldilocks catalysts: computational insights into the role of the 3,3′ substituents on the selectivity of BINOL-derived phosphoric acid catalysts. *J Am Chem Soc*. 2016;138:7910–7917. (b) Reid JP, Ermanis K, Goodman JM. BINOPtimal: a web tool for optimal chiral phosphoric acid catalyst selection. *Chem Commun*. 2019;55:1778–1781.
35. Wang SG, Yin Q, Zhuo CX, You SL. Asymmetric dearomatization of β-naphthols through an amination reaction catalyzed by a chiral phosphoric acid. *Angew Chem Int Ed*. 2015;54:647–650.

36. Changotra A, Das S, Sunoj RB. Reversing enantioselectivity using noncovalent interactions in asymmetric dearomatization of β -naphthols: the power of 3,3' substituents in chiral phosphoric acid catalysts. *Org Lett*. 2017;19:2354–2357.
37. (a) Sharma A, Hartwig JF. Metal-catalyzed azidation of tertiary C–H bonds suitable for late-stage functionalization. *Nature*. 2015;517:600–604. (b) Margrey KA, Czaplyski WL, Nicewicz DA, Alexanian EJ. A general strategy for aliphatic C–H functionalization enabled by organic photoredox catalysis. *J Am Chem Soc*. 2018;140:4213–4217. (c) Le C, Liang Y, Evans RW, Li X, MacMillan DWC. Selective sp^3 C–H alkylation via polarity-match-based cross-coupling. *Nature*. 2017;547:79–83.
38. (a) Jain P, Verma P, Xia G, Yu JQ. Enantioselective amine α -functionalization via palladium-catalysed C–H arylation of thioamides. *Nat Chem*. 2017;9:140–144. (b) Smalley AP, Cuthbertson JD, Gaunt MJ. Palladium-catalyzed enantioselective C–H activation of aliphatic amines using chiral anionic BINOL-phosphoric acid ligands. *J Am Chem Soc*. 2017;139:1412–1415. (c) Yan SB, Zhang S, Duan WL. Palladium-catalyzed asymmetric arylation of $C(sp^3)$ –H bonds of aliphatic amides: controlling enantioselectivity using chiral phosphoric amides/acids. *Org Lett*. 2015;17:2458–2461.
39. Wang H, Tong HR, He G, Chen G. An enantioselective bidentate auxiliary directed palladium-catalyzed benzylic C–H arylation of amines using a BINOL phosphate ligand. *Angew Chem Int Ed*. 2016;55:15387–15391.
40. Bay KL, Yang YF, Houk KN. Computational exploration of a Pd(II)-catalyzed γ -C–H arylation where stereoselectivity arises from attractive aryl–aryl interactions. *J Org Chem* 2018;83:14786–14790.
41. (a) Quasdorf KW, Overman LE. Catalytic enantioselective synthesis of quaternary carbon stereocenters. *Nature*. 2014;516:181–191. (b) Douglas CJ, Overman LE. Catalytic asymmetric synthesis of all-carbon quaternary stereocenters. *Proc Natl Acad Sci USA*. 2004;101:5363–5367.
42. Wang Z, Chen Z, Sun J. Catalytic enantioselective intermolecular desymmetrization of 3-substituted oxetanes. *Angew Chem Int Ed*. 2013;52:6685–6688.
43. Seguin TJ, Wheeler SE. Competing noncovalent interactions control the stereoselectivity of chiral phosphoric acid catalyzed ring openings of 3-substituted oxetanes. *ACS Catal*. 2016;6:7222–7228.
44. (a) Biffis A, Centomo P, Del Zotto A, Zecca M. Pd metal catalysts for cross-couplings and related reactions in the 21st century: a critical review. *Chem Rev*. 2018;118:2249–2295. (b) Cherney AH, Kadunce NT, Reisman SE. Enantioselective and enantiospecific transition-metal-catalyzed cross-coupling reactions of organometallic reagents to construct C–C bonds. *Chem Rev*. 2015;115:9587–9652.
45. (a) Oestreich M. Breaking news on the enantioselective intermolecular heck reaction. *Angew Chem Int Ed*. 2014;53:2282–2285. (b) Li Z, Tong R. Asymmetric total syntheses of (–)-hedycoropyrans A and B. *J Org Chem*. 2017;82:1127–1135.
46. Yasui S, Fujii M, Kawano C, Nishimura Y, Shioji K, Ohno A. Mechanism of dediazonation of arenediazonium salts with triphenylphosphine and trialkyl phosphites. Generation of cation radicals from trivalent phosphorus compounds and their reactions. *J Chem Soc Perkin Trans 2*. 1994;2:177–183.
47. Avila CM, Patel JS, Reddi Y, et al. Enantioselective heck-matsuda arylations through chiral anion phase-transfer of aryl diazonium salts. *Angew Chem Int Ed*. 2017;56:5806–5811.
48. Reddi Y, Tsai CC, Avila CM, Toste FD, Sunoj RB. Harnessing noncovalent interactions in dual-catalytic enantioselective heck–matsuda arylation. *J Am Chem Soc*. 2019;141:998–1009.
49. Humprey GR, Kuethe JT. Practical methodologies for the synthesis of indoles. *Chem Rev*. 2006;106:2875–2911.

50. Fischer E, Hess OO. Synthese von indolderivaten. *Ber Dtsch Chem Ges.* 1884;17:559–568.
51. Müller S, Webber MJ, List B. The catalytic asymmetric Fischer indolization. *J Am Chem Soc.* 2011;133:18534–18537.
52. Seguin TJ, Lu T, Wheeler SE. Enantioselectivity in catalytic asymmetric Fischer indolizations hinges on the competition of π -stacking and CH/ π interactions. *Org Lett.* 2015;17:3066–3069.
53. (a) Trost BM, Crawley ML. Asymmetric transition-metal-catalyzed allylic alkylations: applications in total synthesis. *Chem Rev.* 2003;103:2921–2944. (b) Trost BM, Lee CB. In: Ojima I, ed. *In Catalytic Asymmetric Synthesis II.* Weinheim: Wiley-VCH; 2000:593–650.
54. (a) List B. Introduction: organocatalysis. *Chem Rev.* 2007;107:5413–5415. (b) MacMillan DWC. The advent and development of organocatalysis. *Nature.* 2008;455:304–308. (c) Knowles RR, Jacobsen EN. Attractive noncovalent interactions in asymmetric catalysis: links between enzymes and small molecule catalysts. *Proc Natl Acad Sci USA.* 2010;107:20678–20685.
55. Chen DF, Han ZY, Zhou XL, Gong LZ. Asymmetric organocatalysis combined with metal catalysis: concept, proof of concept, and beyond. *Acc Chem Res.* 2014;47:2365–2377.
56. (a) Brown KA, Kraut J. Exploring the molecular mechanism of dihydrofolate reductase. *Faraday Discuss.* 1992;93:217–224. (b) Allen AE, MacMillan DWC. Synergistic catalysis: a powerful synthetic strategy for new reaction development. *Chem Sci.* 2012;3:633–658.
57. Krautwald S, Sarlah D, Schafroth MA, Carreira EM. Enantio- and diastereodivergent dual catalysis: α -allylation of branched aldehydes. *Science.* 2013;340:1065–1068.
58. Bhaskararao B, Sunoj RB. Origin of stereodivergence in cooperative asymmetric catalysis with simultaneous involvement of two chiral catalysts. *J Am Chem Soc.* 2015;137:15712–15722.